AGU PUBLICATIONS

JGR

Journal of Geophysical Research: Space Physics

RESEARCH ARTICLE
10.1002/2015JA021997

Key Points:
- First particle-in-cell simulation of Ganymede's magnetosphere
- The MHD-EPIC algorithm makes global kinetic simulations affordable
- MHD-EPIC simulation suggests that Galileo observed a flux transfer event during the G8 flyby

Supporting Information:
- Supporting Information S1
- Movie S1

Correspondence to:
G. Tóth,
gtoth@umich.edu

Citation:
Tóth, G., et al. (2016), Extended magnetohydrodynamics with embedded particle-in-cell simulation of Ganymede's magnetosphere, *J. Geophys. Res. Space Physics*, *121*, 1273–1293, doi:10.1002/2015JA021997.

Received 5 OCT 2015
Accepted 17 JAN 2016
Accepted article online 21 JAN 2016
Published online 15 FEB 2016

Extended magnetohydrodynamics with embedded particle-in-cell simulation of Ganymede's magnetosphere

Gábor Tóth[1], Xianzhe Jia[1], Stefano Markidis[2], Ivy Bo Peng[2], Yuxi Chen[1], Lars K. S. Daldorff[3], Valeriy M. Tenishev[1], Dmitry Borovikov[1], John D. Haiducek[1], Tamas I. Gombosi[1], Alex Glocer[3], and John C. Dorelli[3]

[1]Center for Space Environment Modeling, University of Michigan, Ann Arbor, Michigan, USA, [2]Department for Computational Science and Technology, KTH Royal Institute of Technology, Stockholm, Sweden, [3]NASA Goddard Space Flight Center, Greenbelt, Maryland, USA

Abstract We have recently developed a new modeling capability to embed the implicit particle-in-cell (PIC) model iPIC3D into the Block-Adaptive-Tree-Solarwind-Roe-Upwind-Scheme magnetohydrodynamic (MHD) model. The MHD with embedded PIC domains (MHD-EPIC) algorithm is a two-way coupled kinetic-fluid model. As one of the very first applications of the MHD-EPIC algorithm, we simulate the interaction between Jupiter's magnetospheric plasma and Ganymede's magnetosphere. We compare the MHD-EPIC simulations with pure Hall MHD simulations and compare both model results with Galileo observations to assess the importance of kinetic effects in controlling the configuration and dynamics of Ganymede's magnetosphere. We find that the Hall MHD and MHD-EPIC solutions are qualitatively similar, but there are significant quantitative differences. In particular, the density and pressure inside the magnetosphere show different distributions. For our baseline grid resolution the PIC solution is more dynamic than the Hall MHD simulation and it compares significantly better with the Galileo magnetic measurements than the Hall MHD solution. The power spectra of the observed and simulated magnetic field fluctuations agree extremely well for the MHD-EPIC model. The MHD-EPIC simulation also produced a few flux transfer events (FTEs) that have magnetic signatures very similar to an observed event. The simulation shows that the FTEs often exhibit complex 3-D structures with their orientations changing substantially between the equatorial plane and the Galileo trajectory, which explains the magnetic signatures observed during the magnetopause crossings. The computational cost of the MHD-EPIC simulation was only about 4 times more than that of the Hall MHD simulation.

1. Introduction

Ganymede's magnetosphere is unique in the solar system. The Jovian moon is orbiting inside the Jovian magnetosphere, but it has its own intrinsic field that forms a small magnetosphere around Ganymede. The Jovian plasma flows at a subsonic and sub-Alfvénic speed relative to Ganymede, so the moon's magnetosphere produces an Alfvén wing [*Neubauer*, 1998] instead of a bow shock present around planetary magnetospheres. Since the Jovian magnetic field is roughly antiparallel with Ganymede's intrinsic magnetic field at the magnetopause, the configuration of Ganymede's magnetosphere is analogous with the interaction of Earth's magnetosphere with a southward pointing interplanetary magnetic field. Therefore, we expect reconnection concentrated at the upstream tip of the magnetopause and in the magnetotail behind the moon.

The small size of Ganymede's magnetosphere provides a great opportunity to employ our newly developed magnetohydrodynamic with embedded particle-in-cell (MHD-EPIC) model [*Daldorff et al.*, 2014]. Ganymede interacts with the plasma corotating with Jupiter that we refer to as the Jovian wind. The ion inertial length in the Jovian wind with mass density $\rho \approx 56\, m_p/\mathrm{cm}^{-3}$ consisting of a mixture of O^+ and H^+ ions with an average mass $M_i = 14\, m_p$ is about $0.16\, R_G$, where $m_p = 1.67\times10^{-27}$ kg is the proton mass and $R_G = 2634$ km is Ganymede's radius. In comparison, the standoff distance of the magnetopause is about $2\, R_G$, and the tail reconnection is expected to occur within about $4\, R_G$ [*Kivelson et al.*, 1998; *Jia et al.*, 2010; *Jia*, 2015]. Due to the small electron mass M_e, the electron inertial length is much ($\sqrt{M_i/M_e}$ times) smaller than the ion inertial length. Kinetic simulations show, however, that the reconnection process is not very sensitive to the electron mass as long

as $M_i/M_e \geq 100$ [*Ricci et al.*, 2002; *Lapenta et al.*, 2010]. This means that using an artificially increased electron mass of $M_e \sim M_i/100$, the particle-in-cell (PIC) code has a chance to capture even the electron scales.

Previous work on modeling Ganymede's magnetosphere in three dimensions include resistive MHD [*Kopp and Ip*, 2002; *Jia et al.*, 2008, 2009, 2010; *Duling et al.*, 2014], Hall MHD [*Dorelli et al.*, 2015], and multifluid [*Paty and Winglee*, 2004; *Paty et al.*, 2008] simulations. We refer to *Dorelli et al.* [2015] for a more in-depth comparison among these models that all use a fluid description for the plasma. The reconnection physics in these magnetofluid models relies on either Hall resistivity, or ad hoc anomalous resistivity, or simply numerical resistivity. In addition, the distribution function of the ions and electrons is assumed to be Maxwellian. Using a particle-in-cell model therefore can reveal the importance of the kinetic effects, as it captures the microscopic dissipation mechanisms that lead to reconnection based on first principles. Thanks to the Galileo observations [e.g., *Kivelson et al.*, 1997], the models can be not only compared with each other but also validated against in situ measurements of magnetic field.

Although Ganymede's magnetosphere is small, the simulation domain has to be much larger to provide sufficient space for the Alfvén wings and the subsonic and sub-Alfvénic interaction with the Jovian wind. In fact, it is quite challenging to provide proper boundary conditions for subsonic/Alfvénic inflow and outflow. The best approach is to place the boundaries far enough so that Ganymede's effect on the plasma is negligible near the boundaries. We found that it was necessary to make the simulation box about 200 R_G wide in all three directions to make the effects of the boundaries truly insignificant. Doing a pure PIC simulation in such a large domain while resolving at least the ion inertial length would be extremely demanding computationally.

Fortunately, the new MHD-EPIC algorithm provides a feasible alternative: the large computational domain can be efficiently modeled with the Hall MHD code, while the vicinity of the moon, where kinetic effects are potentially important, is modeled with the PIC code. The Hall MHD and PIC models are two way coupled to ensure the consistency of the solution. The MHD-EPIC algorithm can provide a global time-dependent solution where all the critical dynamics is handled by the PIC code. As we will show in this paper, the MHD-EPIC model provides a solution that is similar to but significantly different from the Hall MHD solution reported by *Dorelli et al.* [2015].

The computational models and the simulation setup are described in section 2, the main simulation results and comparison with measurements are presented in section 3, additional simulations are described in section 4, and we conclude with section 5.

2. Model Description

This paper presents the first three-dimensional (3-D) application of the recently developed Hall magnetohydrodynamic with embedded particle-in-cell (MHD-EPIC) model [*Daldorff et al.*, 2014]. The Hall MHD equations are solved by the BATS-R-US code [*Powell et al.*, 1999; *Tóth et al.*, 2008], while the embedded PIC regions are simulated by the iPIC3D code [*Markidis et al.*, 2010]. The two codes are coupled together in the Space Weather Modeling Framework (SWMF) [*Tóth et al.*, 2005, 2012]. This section describes the models and the coupling in some detail. We concentrate on the particular algorithms and settings used in the Ganymede simulations.

2.1. Hall Magnetohydrodynamic Model: BATS-R-US

Block-Adaptive-Tree-Solarwind-Roe-Upwind-Scheme (BATS-R-US) is a flexible global MHD code that has been extensively used to study plasma interactions with a variety of solar system bodies including planets, planetary moons, and comets. BATS-R-US allows adaptive mesh refinement in combination with curvilinear coordinates. For the simulations here, an adaptive Cartesian grid is employed in a $-128\,R_G < x, y, z < 128\,R_G$ cube in the GphiO coordinates centered around Ganymede. The X axis points in the direction of the Jovian wind, the Z axis is parallel to the Jovian rotational axis, and the Y axis completes the coordinate system pointing approximately toward Jupiter. The smallest cell size is $1/32\,R_G$ in a box $-3\,R_G < x < 4\,R_G$, $-3\,R_G < y < 3\,R_G$, and $-2\,R_G < z < 2\,R_G$ and gradually coarser farther away up to $4\,R_G$ cells. The total number of BATS-R-US grid cells is about 8.5 million.

The moon is represented by a spherical inner boundary at radial distance $1\,R_G$. We apply absorbing boundary conditions here: if the plasma velocity points toward the surface, then a zero gradient is applied, while if the velocity is pointing away from the surface, then the radial component of the velocity is reversed. The transverse components of the velocity, the density, and the pressure always have zero gradients. The magnetic field $\mathbf{B}$ is split into the intrinsic dipole field $\mathbf{B}_0$ and the deviation $\mathbf{B}_1$. The $\mathbf{B}_0$ field is calculated analytically

from a magnetic dipole pointing approximately in the $-Z$ direction with 719 nT field strength at the equator [*Kivelson et al.*, 2002]. The magnetic axis is tilted by 4.37° relative to the Z axis, and it intersects the surface at 289° longitude on the Northern Hemisphere. The boundary condition is zero gradient for the transverse components of $\mathbf{B}_1$ and reflective for the radial component of $\mathbf{B}_1$. These inner boundary conditions are crucial for obtaining the correct size (that is consistent with Galileo data) for the magnetosphere.

In this paper, we focus on comparing our model results with Galileo observations obtained during the G8 flyby that passed through the upstream magnetopause and thus it is the most relevant for looking at kinetic effects. The G8 flyby took place when Ganymede was located near the center of Jupiter's plasma sheet, so at the outer boundaries all the MHD quantities are fixed to the corresponding Jovian wind values following *Jia et al.* [2008]: mass density $\rho = 56 m_p/\mathrm{cm}^{-3}$, velocity $u_x = 140$ km/s, magnetic field $\mathbf{B} = (0, -6, -77)$ nT, and total plasma pressure $p = 3.8$ nPa from which the ion pressure is $p_i = 3.17$ nPa and the electron pressure is $p_e = p_i/5 = 0.63$ nPa. The ion mass is taken to be the average $M_i = 14\, m_p$. Using fixed boundary conditions for all variables is an overspecification from the mathematical point of view, but it works well numerically as long as the outer boundaries are far enough from Ganymede. Simple fixed inflow and zero-gradient outflow boundary conditions (typically used for the solar wind around planetary magnetospheres) do not work for the subsonic and sub-Alfvénic Jovian wind.

It is important to check if the grid resolution is sufficiently fine to correctly respresent the modeled physics. The ion inertial length in the Jovian wind is $d_i = c/\omega_{pi} = c/(1320\sqrt{n/M_i})$, where c is the speed of light, $n = 4$ is the number density in cm^{-3} units, and $M_i = 14$ is the ion mass in proton mass. We get $d_i \sim 425$ km $\sim 0.16\, R_G$ that is resolved by about five to six grid cells of size $\Delta x = 1/32\, R_G = 82.3$ km. Another way to see if the Hall term $\mathbf{B} \times \mathbf{J}/(ne)$ matters in the induction equation is to compare the maximum value of the Hall velocity $u_H = \mathbf{J}/(ne)$ with the typical bulk velocity of the plasma, where $e = 1.6 \times 10^{-19}$ C is the elementary charge. Given the magnetic field strength $B \sim 100$ nT and grid resolution $\Delta x = 1/32\, R_G$, the maximum current density is $J \sim (1/\mu_0)B/\Delta x \sim 10^{-6}$ A/m^2, so the maximum value of the Hall velocity is $u_H \sim 1500$ km/s, which greatly exceeds the bulk velocity.

In addition to the Hall term, the electron pressure gradient term $\nabla p_e/(ne)$ is also included in the generalized Ohm's law. In this paper the electron pressure is simply taken to be a fixed fraction (one fifth) of the ion pressure in the BATS-R-US model. The main significance of this particular choice is that the electron pressure is passed to the PIC code at the boundaries of the PIC region, and we wish to keep the electron thermal speed comparable to the ion thermal speed in the PIC code given the $M_e \sim M_i/100$ choice for the electron mass. This matters because the implicit PIC time step is limited by the electron thermal velocity divided by the cell size. While setting the electron pressure this way is somewhat arbitrary, in essence it states that the plasma pressure is dominated by the ions, which is not inconsistent with the plasma observations [*Kivelson et al.*, 2004]. In future work we will solve the electron pressure equation in the MHD code instead of using a fixed fraction.

To speed up the BATS-R-US calculation, the Hall effect is restricted to the $|x| < 4\, R_G$, $|y| < 3\, R_G$, and $|z| < 2\, R_G$ box centered around the moon. Outside this region the ideal MHD equations are solved, which is a good approximation, since the currents are weak far from the moon, so the Hall velocity u_H is very small.

The time discretization employs the explicit-implicit time stepping scheme [*Tóth et al.*, 2006] with a fixed time step $\Delta t = 0.025$ s. The spatial discretization is based on the second-order accurate Rusanov scheme with Koren's third-order limiter. To further reduce numerical diffusion while maintaining good convergence for the implicit solver, only 10% of the whistler wave speed is taken into account for the maximum wave speed that is used in the numerical flux of the Rusanov scheme [*Tóth et al.*, 2008]. The numerical divergence of the magnetic field is controlled with the eight-wave scheme [*Powell*, 1994]. In some cases we found that an additional hyperbolic cleaning [*Dedner et al.*, 2003] improves the magnetic field solution across the MHD-PIC interface.

2.2. Implicit Particle-in-Cell Model: iPIC3D

In the embedded kinetic regions the solution is obtained by the implicit particle-in-cell code iPIC3D [*Markidis et al.*, 2010]. iPIC3D solves the full set of Maxwell's equations for the electromagnetic fields, coupled with the equations of motion for electrons and ions on uniform 3-D Cartesian grids. In the Ganymede simulations the cell size is $\Delta x = 1/32\, R_G \sim 82.3$ km in all PIC regions and the time step $\Delta t = 0.025$ s is the same as for BATS-R-US. The implicit PIC method is accurate as long as $\Delta x/\Delta t \sim 3300$ km/s is larger than the electron thermal speed, which is satisfied in the simulations. We note that unlike explicit PIC, the implicit PIC method remains stable against the finite grid instability even if the grid does not resolve the Debye length.

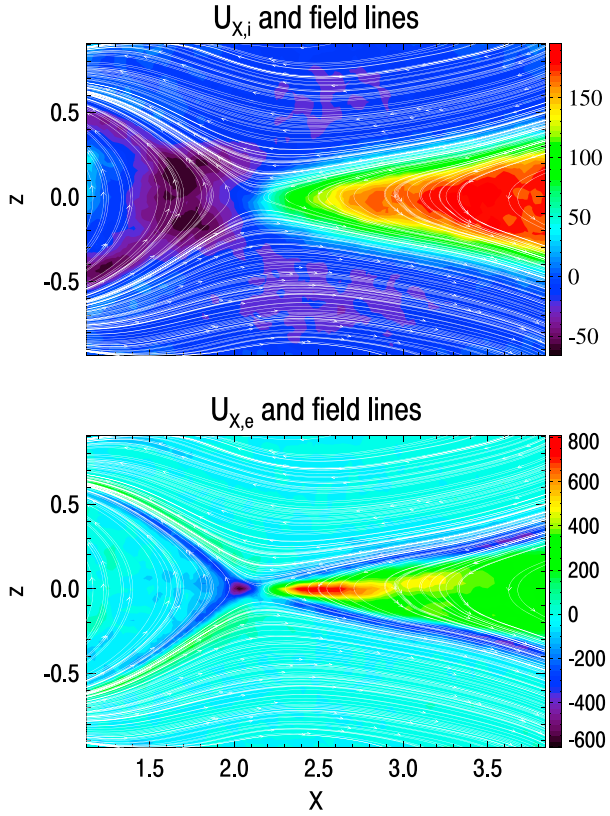

Figure 1. Meridional cut through the tail PIC region showing the X components of the (top) ion and (bottom) electron bulk velocities in km/s and the magnetic field lines (white lines). The coordinates are given in units of Ganymede radius R_G. The electron jets extending from the X line are clearly visible. Note that the color scales are different for the two panels.

Initially, there are $N_i = 216$ ions and $N_e = 216$ electron macroparticles per grid cell. As the simulation progresses, the particles can freely move in the PIC regions. When a particle goes through the boundary, it is simply lost. On the other hand, the ghost cells surrounding the PIC regions are filled in with N_i ions and N_e electrons every time step, and these particles can move into the domain. The total number of particles can vary somewhat during the run, but it typically remains close to the original number. The ratio of ion and electron particle masses is set to $M_i/M_e = 100$, which is sufficiently large to produce realistic reconnection dynamics. This means that the electron skin depth $d_e = d_i/\sqrt{M_i/M_e} \sim 0.018\,R_G$, which is about half of the cell size Δx. Figure 1 shows the X components of the ion and electron bulk velocities on the $y = 0$ plane inside the tail PIC region. The electron jets emanating from the X line of the reconnection are reasonably well resolved as shown by the red and magenta regions in Figure 1 (bottom). Note that the electron velocity is much larger than the ion velocity. The figure suggests that while details at the electron scale are probably not accurate, the overall reconnection dynamics should still be well captured.

2.3. MHD-EPIC Coupling Within the Space Weather Modeling Framework

The BATS-R-US and iPIC3D models have been integrated into and coupled through the Space Weather Modeling Framework (SWMF). Both models are compiled into a single executable, and they are initialized, advanced, and coupled under the control of the SWMF. Both models are massively parallel. In the Ganymede runs, BATS-R-US and all instances of iPIC3D use all 960 CPU cores that the simulations were run with.

The MHD-EPIC algorithm has been described in detail by *Daldorff et al.* [2014]. Here we describe the main idea and the new features and developments. First, we obtain an approximate steady state solution by running BATS-R-US in local time step mode (each grid cell is advanced with the locally stable time step) for 100,000 time steps in the full computational domain (see Figure 2). Then we restart the SWMF and specify the location of the PIC regions.

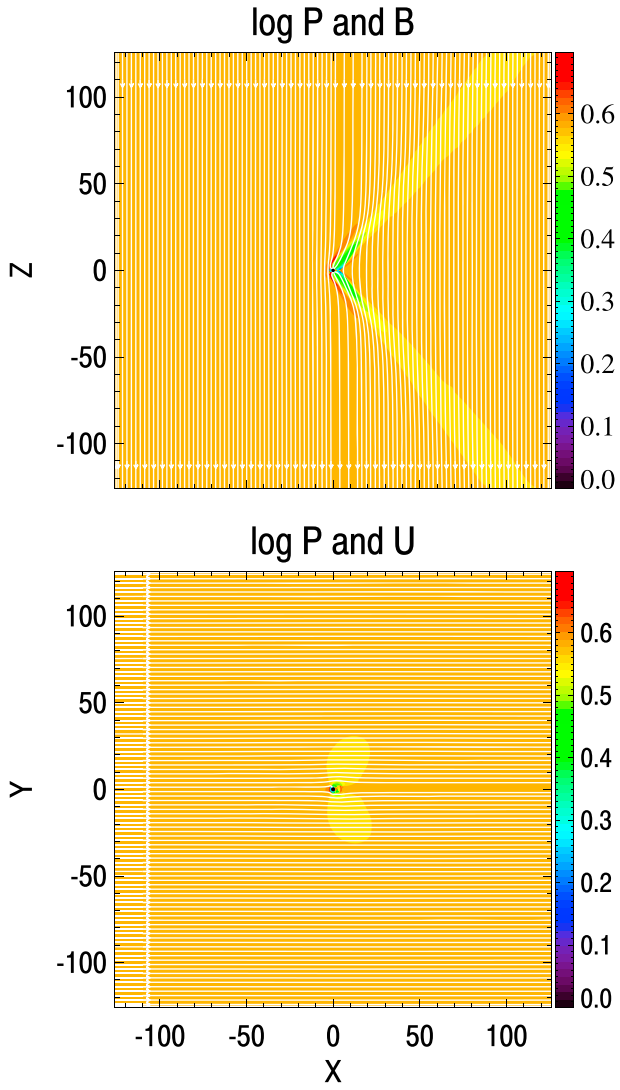

Figure 2. (top) Meridional and (bottom) equatorial cuts showing the Hall MHD solution in the full computational domain. The white lines show the magnetic field lines (Figure 2, top) and streamlines (Figure 2, bottom), respectively. The color shows the 10 based logarithms of pressure in unit of nanopascal. The Alfvén wings and slow wave generated by Ganymede in the subsonic and sub-Alfvénic Jovian wind are clearly seen in the meridional cut. Note that the solution is essentially unperturbed near the outer boundaries.

At the beginning of the first time step of the restarted run, BATS-R-US sends the MHD solution inside and around the PIC regions to iPIC3D, and iPIC3D initializes the ion and electron macroparticles with Maxwellian distributions that have the same mass, momentum, and energy density as the MHD solution. From charge neutrality the number densities of the electrons and ions are taken to be equal and obtained from the MHD mass density ρ as $n_i = n_e = \rho/(M_i+M_e)$. The ion and electron velocities $\mathbf{u}_i$ and $\mathbf{u}_e$ are obtained from the following equations: (1) the total momentum $M_i n_i \mathbf{u}_i + M_e n_e \mathbf{u}_e$ is equal to the $\rho\mathbf{u}$ momentum of the MHD state and (2) the current density derived in the MHD code as $\mathbf{J} = (1/\mu_0)\nabla \times \mathbf{B}$ is equal to $ne(\mathbf{u}_i - \mathbf{u}_e)$. The ion and electron pressures are obtained from the total MHD pressure p. Since in these simulations the MHD code does not solve for electron pressure, we take $p_e = 0.2p_i$ and require that $p = p_e + p_i$. The ion and electron macroparticles are then generated in each PIC computational cell with the algorithm detailed by *Daldorff et al.* [2014]. The magnetic field **B** is simply taken from the MHD solution by the PIC code, and the electric field is calculated as $\mathbf{E} = -\mathbf{u}_e \times \mathbf{B}$, which properly includes the Hall effect.

In subsequent time steps BATS-R-US still sends the MHD solution to iPIC3D, but it is only used to generate particles in the ghost cells surrounding the PIC regions. On the other hand, iPIC3D calculates the MHD quantities

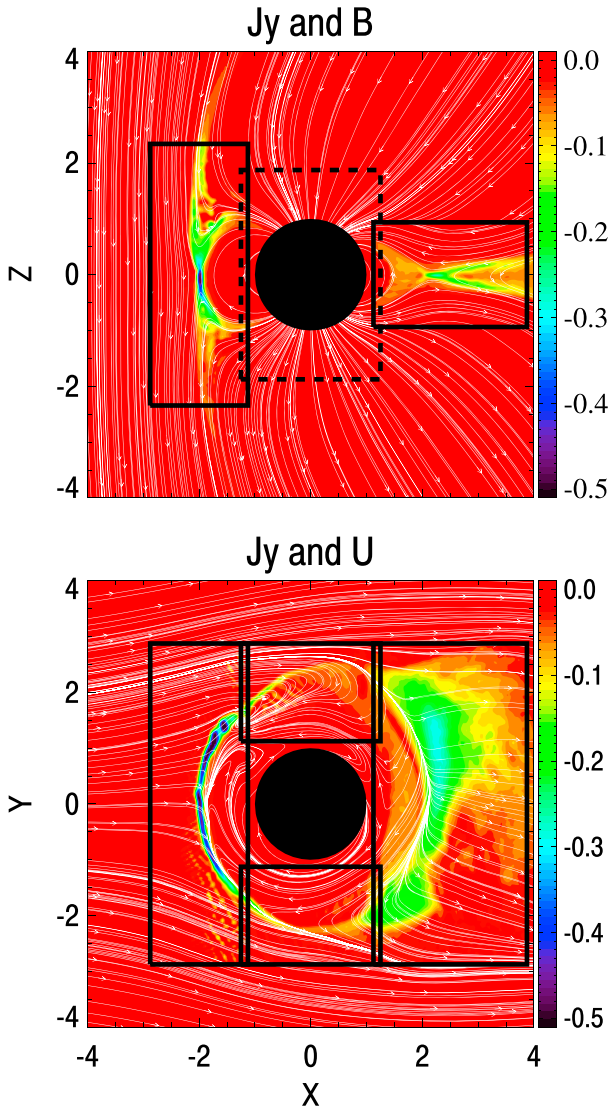

Figure 3. (top) Meridional and (bottom) equatorial cuts showing the location of the PIC regions (black rectangles). The white lines represent the magnetic field lines (Figure 3, top) and streamlines (Figure 3, bottom), respectively. The colors show the *Y* component of the current density in units of $\mu A/m^2$.

(mass density, momentum, and pressure) inside the PIC regions and sends them together with the magnetic field to BATS-R-US, so that the MHD solution can be overwritten by the PIC solution inside the PIC regions.

To facilitate the Ganymede simulations (and future MHD-EPIC applications), we have developed a new general coupler in the SWMF to perform an efficient parallel coupling algorithm that uses direct Message Passing Interface data transfer between the BATS-R-US and iPIC3D processes. The new coupler works for arbitrary 2-D and 3-D grids, and it does not require the BATS-R-US and iPIC3D grids to be aligned or have the same grid resolution. The implementation now also allows multiple PIC regions. We have also implemented a new *tight coupling* option into the SWMF, where the two models are coupled every time step and the length of the possibly varying time step is determined by the *master* component (in this case BATS-R-US) and it is sent to the *slave* component (in this case iPIC3D) so that the two models take the same time step. The tight coupling allows the two models to remain fully in sync, which makes the solution at the coupling interface more accurate and robust.

In the MHD-EPIC simulations of Ganymede's magnetosphere we use four PIC regions that surround Ganymede but still cover all the potential reconnection sites as shown in Figure 3. This is necessary, because the current version of iPIC3D cannot handle internal boundaries, so the PIC regions cannot intersect with the surface of

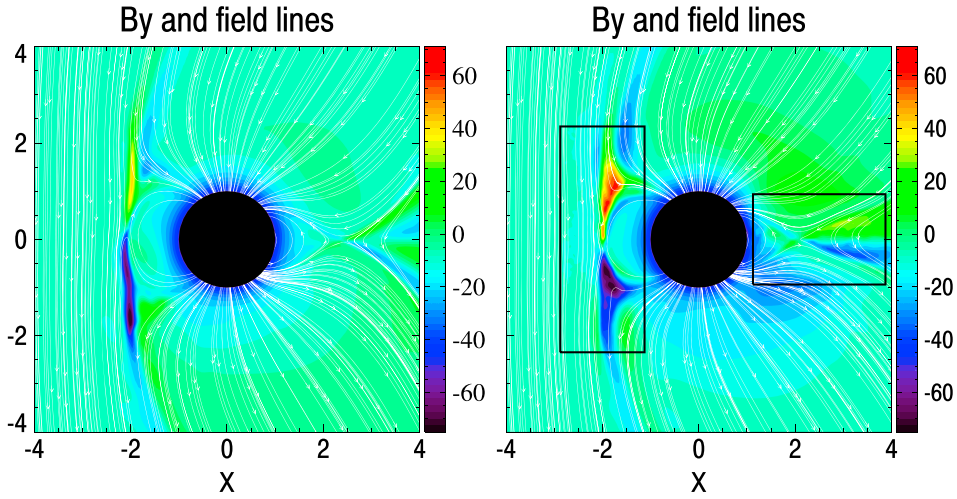

Figure 4. Meridional cuts of the (left) Hall MHD and (right) Hall MHD-EPIC solutions at $t = 350$ s. The white lines trace the B_x and B_z components of the magnetic field. The colors show the out-of-plane component B_y in units of nanotesla. The black rectangles indicate the edges of the upstream and downstream PIC regions.

the moon at $r = 1\,R_G$. In units of R_G the upstream PIC region is placed at $x \in [-2.875, -1.125]$, $|y| < 2.875$, and $|z| < 2.34375$. The tail region is at $x \in [1.125, 3.875]$, $|y| < 2.875$, and $|z| < 0.9375$. Finally, the two flank regions are at $|x| < 1.25$, $y \in [\pm 1.125, \pm 2.875]$, and $|z| < 1.875$ corresponding to the plus and minus signs, respectively. Given the $\Delta x = 1/32\,R_G$ grid resolution in iPIC3D, the four regions consist of $56 \times 184 \times 150 \sim 1.5$ million (upstream), $88 \times 184 \times 60 \sim 1$ million (tail), and twice $80 \times 56 \times 120 \sim 0.5$ million (flanks) grid cells. The approximately 3.6 million PIC cells are initially filled with 216 ion and 216 electron macroparticles per cell, which results in about 1.55 billion particles in total.

Although the four PIC regions slightly overlap at $x \in [\pm 1.125, \pm 1.25]$, currently, there is no direct communication among the PIC regions, so all information is going through the MHD-EPIC coupling. This means that the distribution functions are set to be Maxwellian at these boundaries just like at the other boundaries of the PIC regions. Since the main reconnection sites are fully covered by the upstream and tail regions, the lack of direct coupling between the PIC regions does not have a significant influence on the overall solution.

3. Results

We ran two simulations starting from the quasi steady state solution obtained with the Hall MHD code. The first simulation simply continued the run with Hall MHD in time accurate mode, while the second simulation employed the Hall MHD-EPIC model with the four embedded PIC regions. Both simulations were continued for 10 min of physical time, which is sufficient for the small magnetosphere to evolve into a quasiperiodic dynamics. The simulations could be run longer if needed, and we, in fact, performed longer runs up to 20 min. The simulations do not exhibit accumulation of numerical errors: the total mass, momentum, and energy do not change significantly during the runs.

3.1. Comparison of Hall MHD and Hall MHD-EPIC simulations

Figure 4 shows the Hall MHD and the Hall MHD-EPIC solutions at time $t = 350$ s. The white lines are traces of the B_x and B_z components of the magnetic field, while the colors show the out-of-plane B_y component. The figure confirms that the reconnection sites are fully inside the upstream and tailside PIC regions shown by the black rectangles in the right panel. This means that the reconnection is fully modeled by iPIC3D in the MHD-EPIC simulation. The solution goes smoothly through the boundaries of the PIC regions thanks to the two-way coupling with the MHD-EPIC algorithm.

The two solutions are clearly similar in terms of the overall configuration of the magnetosphere, but there are also significant differences. Both models show the field signature typical of Hall reconnection near the upstream and tail reconnection sites. On the upstream side the PIC solution (Figure 4, right) shows a wider area with $|B_y| > 50$ nT than the Hall MHD result (Figure 4, left). We confirmed that this difference does not disappear even if both models are run with twice finer grid resolution.

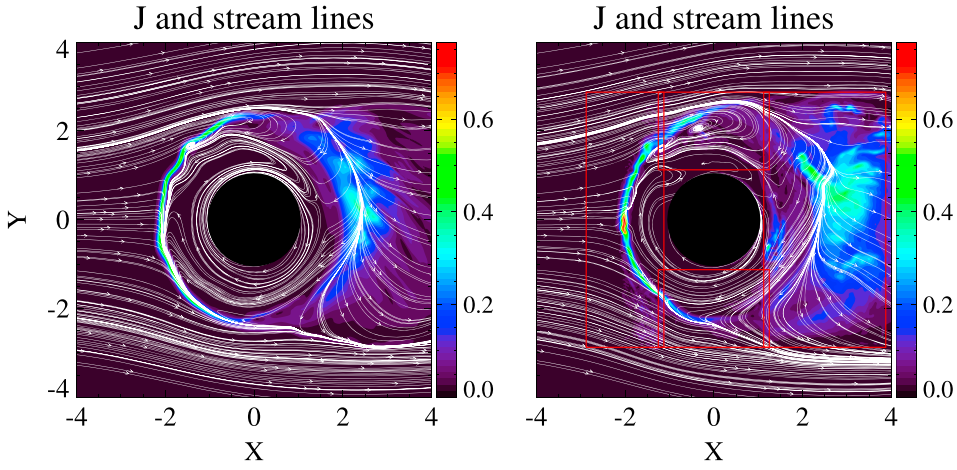

Figure 5. Equatorial cuts of the (left) Hall MHD and (right) Hall MHD-EPIC solutions at $t = 350$ s. The white lines trace the u_x and u_y components of the velocity. The colors show the magnitude of the current density J in units of μA/m^2. The red rectangles indicate the edges of the four PIC regions.

The PIC solution produces many flux transfer events (FTEs) at the upstream magnetopause during the 10 min simulation as shown in the movie provided in the online material. This quasiperiodic FTE production is similar to that obtained by *Jia et al.* [2010] using anomalous resistive MHD simulations. One of these events near the nose of the magnetopause is captured in Figure 4 (right). Interestingly, the Hall MHD simulation is much less dynamic, as it only produces very small islands at the dayside reconnection site. We note, however, that the FTE formation in the Hall MHD solution strongly depends on the grid resolution (this will be discussed in section 4). Figure 5 shows the current density and velocity streamlines in the equatorial frame in a similar format as Figure 2 in *Dorelli et al.* [2015] although the coordinate systems are flipped. Both simulations show a pronounced asymmetry with respect to the $\pm Y$ direction similar to that found by *Dorelli et al.* [2015] in their Hall MHD simulations but not in their resistive MHD solution. This confirms that the asymmetry is a consequence of the Hall physics that is captured by both the Hall MHD and the kinetic PIC simulations. The Hall MHD solution shows clear signatures of the Kelvin-Helmholtz (KH) instability in the $-X, +Y$ quadrant of the magnetopause. The PIC solution also has small ripples in the same part of the magnetopause, but the wavelength and the amplitude are smaller than those in the Hall MHD solution. It is likely that the difference is due to kinetic effects, such as finite Larmor radius, not captured by the Hall MHD scheme. We note that KH observations at Mercury show similar dawn-dusk asymmetry [*Liljeblad et al.*, 2014].

Although the magnetic field structures of the two simulations look quite similar, some of the plasma parameters, such as density and pressure, are quite different. Figures 6 and 7 show the density and pressure in the meridional and equatorial cut planes. Inside the magnetosphere, especially on the tailside, the density is much smaller in the Hall MHD simulation than in the MHD-EPIC simulation. The MHD-EPIC solution shows a density peak with $\rho > 70$ amu/cm^3 on the moon side of the tail reconnection. The Hall MHD solution does not have a similar feature. In the MHD-EPIC simulation the pressure is reduced in the closed field line region on the upstream side and increased on the tailside compared to the Hall MHD simulation. The MHD-EPIC pressure shows a similar enhancement as the density on the tailside. This is likely a result of the reconnection jet hitting the closed field lines. The Hall MHD pressure is also enhanced slightly but with much smaller values. These comparisons show that Hall MHD and PIC produce significantly different solutions in the regions affected by the magnetic reconnection. These differences are not sensitive to grid resolution (see section 4).

3.2. Comparison With Galileo Magnetic Field Measurements

While comparing the Hall MHD and PIC solutions provides insight into the importance of kinetic effects, it is even more important to make sure that the simulations are consistent with measurements. This section compares the simulations with the magnetic data obtained during the Galileo G8 flyby on 7 May 1997. Figure 8 compares measured (black line) and simulated (blue line) magnetic fields extracted from the MHD-EPIC simulation at an arbitrary fixed simulation time ($t = 99$ s). The observation time on the horizontal axis is measured in minutes relative to 00 UT of 7 May 1997. Clearly, there is a discrepancy, especially in the B_x component. The agreement can be improved substantially if the data are extracted from a modified trajectory that is obtained

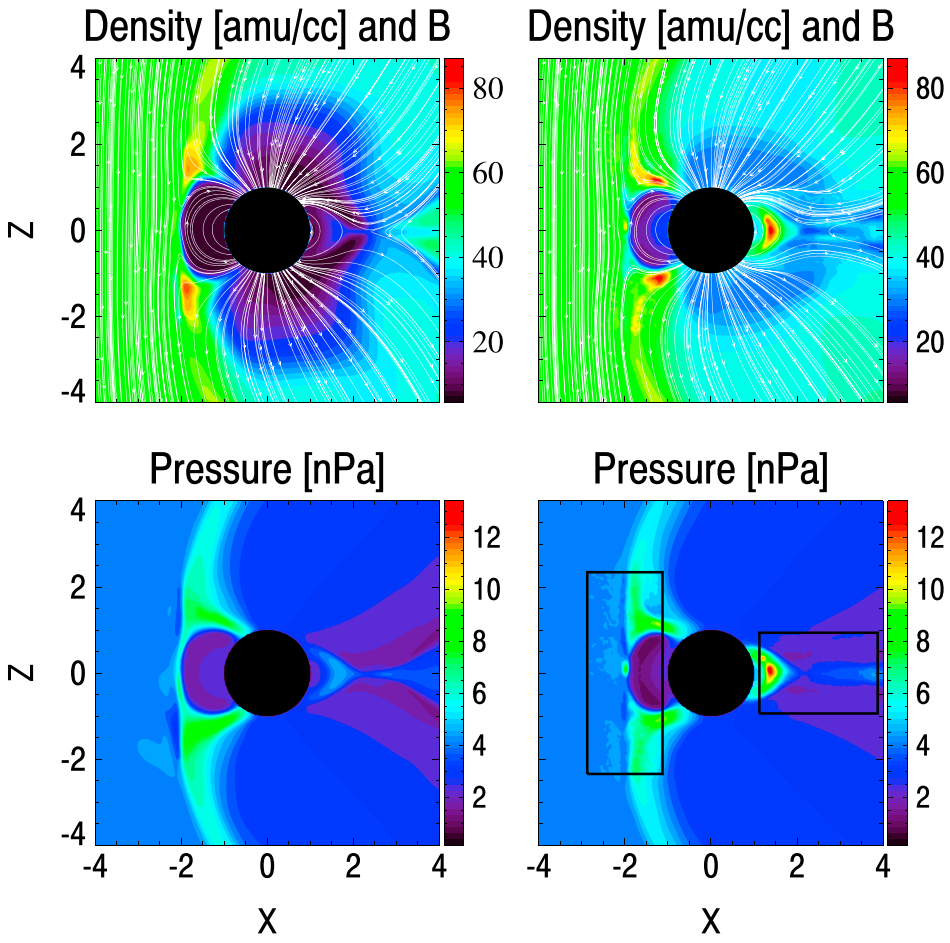

Figure 6. Meridional cuts of the (left column) Hall MHD and (right column) Hall MHD-EPIC solutions at $t = 350$ s showing the (top row) mass density and (bottom row) pressure. The black rectangles in Figure 6 (bottom right) indicate the edges of the upstream and downstream PIC regions for the MHD-EPIC simulation.

by multiplying the trajectory coordinates by 1.06. This corresponds to a radial stretching by 6%. The magnetic field extracted along the stretched trajectory is shown by the red line, which agrees quite well with the observations. This means that the simulated magnetosphere is slightly larger than it should be. This is most likely caused by the inner boundary conditions that provide a rather crude representation of the electric resistivity of the moon. We note that *Dorelli et al.* [2015] applied a similar adjustment (an outward offset by 0.05 R_G in the x and z directions) to improve the agreement with observations.

The optimal stretching factor was determined by minimizing the difference between the measured and simulated magnetic field components inside the magnetosphere (between 952 min and 962 min observation times). For the MHD-EPIC simulation the optimal stretching factor is $s = 1.06$ resulting in an average difference of $|\Delta B_{xyz}| = 12.5$ nT. For the Hall MHD simulation the optimal value is at $s = 1.08$ with $|\Delta B_{xyz}| = 14.7$ For sake of simplicity we use $s = 1.06$ for both models noting that this results in a moderate increase in $|\Delta B_{xyz}|$ to 15.6 nT for the Hall MHD simulation.

We continue our data comparison by using the radially stretched (by 6%) trajectory and concentrate on the shape of the magnetic signatures. Due to the dynamic and somewhat chaotic nature of the reconnection process, one cannot hope to produce a point-to-point match with Galileo observations. Our simulations cover 10 min physical time, which is long compared to the dynamic time scales but shorter than the duration of the flyby: Galileo measured clear magnetic signatures due to Ganymede's magnetosphere for about 15–20 min. To make a meaningful comparison with Galileo, we have stacked the simulations repeatedly to cover the whole flyby. For any given observation time t_{obs} we calculate the corresponding simulation time as

$$t_{sim} = t_{sim,0} + \text{modulo}(t_{obs} - t_{obs,0}, t_{sim,1} - t_{sim,0}) \quad (1)$$

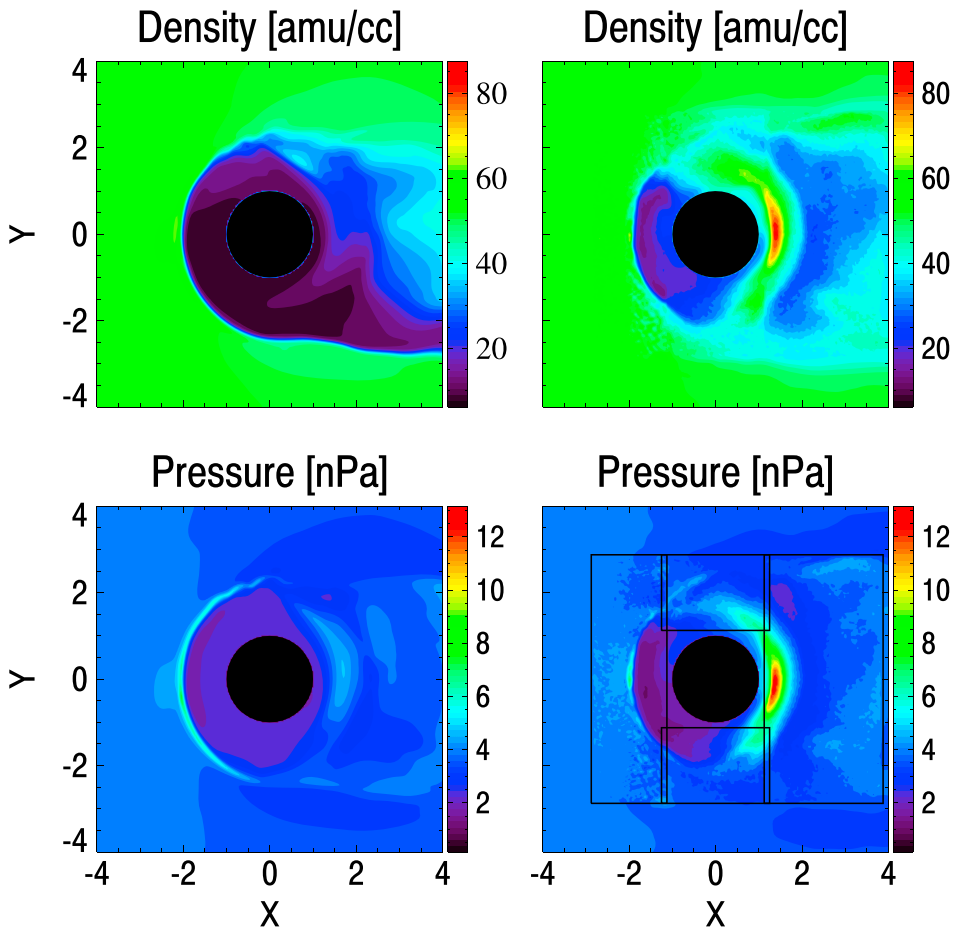

Figure 7. Equatorial cuts of the (left column) Hall MHD and (right column) Hall MHD-EPIC solutions at $t = 350$ s showing the (top row) mass density and (bottom row) pressure. The black rectangles in Figure 7 (bottom right) indicate the edges of the four PIC regions for the MHD-EPIC simulation.

where $t_{obs,0}$ is the reference observation time, which is essentially a free parameter. The start time $t_{sim,0}$ is set to 60 s so that the initial transients (going from the approximate steady state into the time accurate simulation) are not included. The final time is $t_{sim,1} = 600$ s, so we use the remaining 9 min for both simulations. We note that the simulations could be continued longer than 10 min, but that would not add much extra information. Instead, we used the limited computational resources to do multiple runs with different parameters as discussed in section 4.

Figures 9 and 10 show the Galileo observations compared with data extracted from the Hall MHD and MHD-EPIC simulations using $t_{obs,0} = 952.75$ min. The crosses in the bottom panels show where $t_{sim} = t_{sim,0}$. While the Hall MHD simulation shows a reasonable agreement with the smooth variation of the observed data, the small time scale variations are quite different. The Hall MHD solution shows a high frequency (about 10 s period) oscillation with fairly small amplitude between 948 min and 953 min observation times corresponding to the inbound magnetopause crossing. The solution is relatively smooth through the outbound magnetopause crossing. In contrast, the measured magnetic field varies on time scales ranging from seconds to about a minute or two. Figure 10 shows that the MHD-EPIC solution matches the observed variations much better, especially around the outbound magnetopause crossing between 960 min and 965 min. Both the time scales and amplitudes agree reasonably well.

The Galileo data show a large amplitude (about 100 nT in the B_z component) and 1 min wide signal between $t_{obs} = 962$ min and 963 min. Figure 11 shows a cut plane at $Z = 0.83\,R_G$ through the MHD-EPIC simulation at $t_{sim} = 190\,s$, which approximately corresponds to where the outbound B_z peak is found in the synthetic

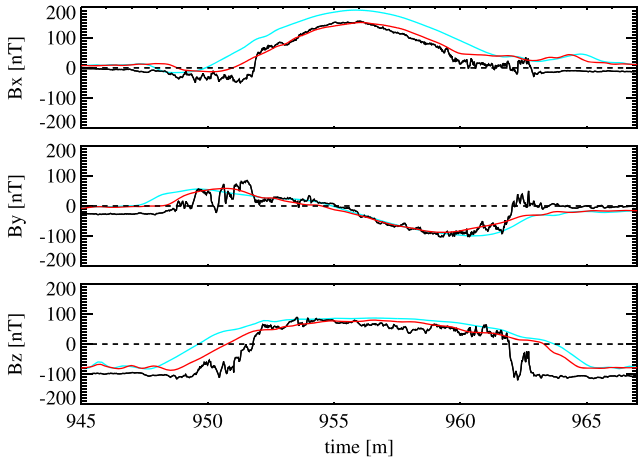

Figure 8. Comparison of the observed (black line) and simulated (blue line) magnetic fields along the Galileo trajectory at an arbitrary simulation time (400 s) in the MHD-EPIC simulation. The red line shows the simulated values along a slightly modified trajectory that is obtained from the original by multiplying the trajectory coordinates with 1.06. The observation time on the horizontal axis is measured in minutes relative to 00 UT of 7 May 1997.

satellite data as shown in the bottom panel of Figure 10 at $t_{obs} \approx 964$ min. Galileo's actual trajectory is shown with the dashed black line, while the stretched trajectory, where the data are extracted from the simulation, is shown by the solid black line. The $Z = 0.82\,R_G$ value is 1.06 times the z coordinate of the actual trajectory, which was approximately 0.77 R_G at this time. There is a wound up field in the B_x and B_y components along the stretched trajectory at around $y = 1.3\,R_G$. Figure 12 shows a 3-D visualization of the magnetic field lines (colored with pressure) at the same time from two different view points. The magnetic field lines form two separate flux ropes, one of them intersecting Galileo's trajectory shown by the gray tube. This flux rope is approximately perpendicular to the meridional ($Y = 0$) plane where it is near the equatorial plane ($Z = 0$), but at the intersection with the Galileo trajectory ($Z \approx 0.8$) its direction changes by almost 90°, so it is roughly aligned with the Z axis. This explains why the B_x and B_y components are wound up in the $Z = 0.82$ plane shown in Figure 11.

The 3-D field line structure clearly indicates that the MHD-EPIC simulation produced a flux transfer event (FTE). Figure 13 shows a comparison of the Galileo data and the MHD-EPIC results zoomed in for the outbound time interval (same curves were shown in Figure 10 for a longer time interval). Galileo crossed the

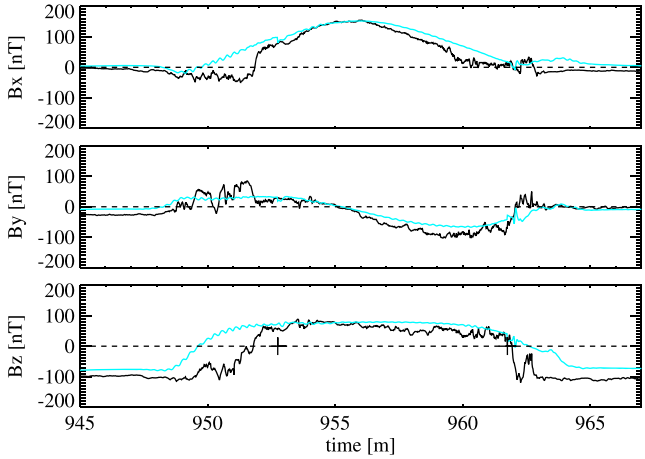

Figure 9. Comparison of the observed (black line) and Hall MHD (blue line) magnetic fields. The time series is extracted from the simulation that is repeated in a periodic fashion. The starting points of the periods are indicated by the crosses in the bottom panel.

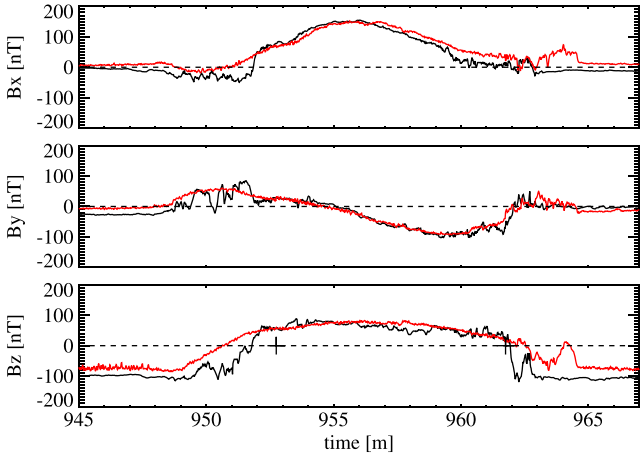

Figure 10. Comparison of the observed (black line) and Hall MHD-EPIC (red line) magnetic fields. The time series is extracted from the simulation that is repeated in a periodic fashion. The starting points of the periods are indicated by the crosses in the bottom panel.

magnetopause at around 961.9 min, while in the simulation the crossing occurs at about 962.5 min as shown by the B_z crossing from positive to negative values. About 0.3 min after the crossing the B_x component rises by about 50 nT from a minimum of −20 nT for Galileo and −10 nT for the simulation, respectively. The B_x curves remain positive for about 0.5 min in the Galileo observations and about 1.5 min in the simulation. During the same interval, the B_y components are mostly positive with some oscillations between 0 and 50 nT. In both cases, the B_z component has a large peak in the last minute of the event with an amplitude of about 100 nT relative to the value outside the magnetosphere, which is −110 nT and −70 nT in the Galileo data and the MHD-EPIC results, respectively. Although we cannot expect quantitative agreement, the similarities between the observed and simulated magnetic features are quite striking. Based on the overall similarities, we conclude that Galileo has most likely observed a flux transfer event during the outbound magnetopause crossing in this flyby.

To make the comparisons somewhat more quantitative, we calculated the power spectrum of the Galileo data and the time series extracted from the two simulations with the same parameters that were used for Figures 9 and 10. Figure 14 shows the comparison of the power spectra of the three components of the magnetic field. The frequency range is shown up to 0.3 Hz, because shorter frequencies are not meaningful given the discrete time resolution (the model output is saved at every second of simulation time). The agreement between the Galileo and MHD-EPIC power spectra is excellent, while the Hall MHD power spectra are quite different, with much less power in the higher frequencies.

4. Additional Simulations

We made several additional runs to check how the results depend on various parameters. Here we briefly describe these runs and the conclusions made from them with respect to the reference Hall MHD and Hall MHD-EPIC runs presented in the previous section. A more in-depth analysis and additional runs are deferred to a future paper.

We tried an MHD-EPIC simulation with BATS-R-US solving the ideal MHD (instead of Hall MHD) equations. Although the simulation worked for a reasonably long period, eventually, an instability developed at the MHD-PIC boundary and the iPIC3D code crashed with unphysically large pressure and correspondingly large thermal velocities. We do not conclude that Hall MHD is a requirement for MHD-EPIC, but it seems to matter whether the PIC region is coupled with an ideal or a Hall MHD code.

As shown in the previous section, the pure Hall MHD reference simulation showed much smoother results than the MHD-EPIC simulation. A possible reason for this can be the numerical diffusion due to the finite grid resolution. We did a high-resolution Hall MHD run with 1/64 R_G grid resolution near the moon using about 50 million grid cells in total. The time step was reduced to $\Delta t = 0.01$ s (from 0.025 s). The overall large-scale

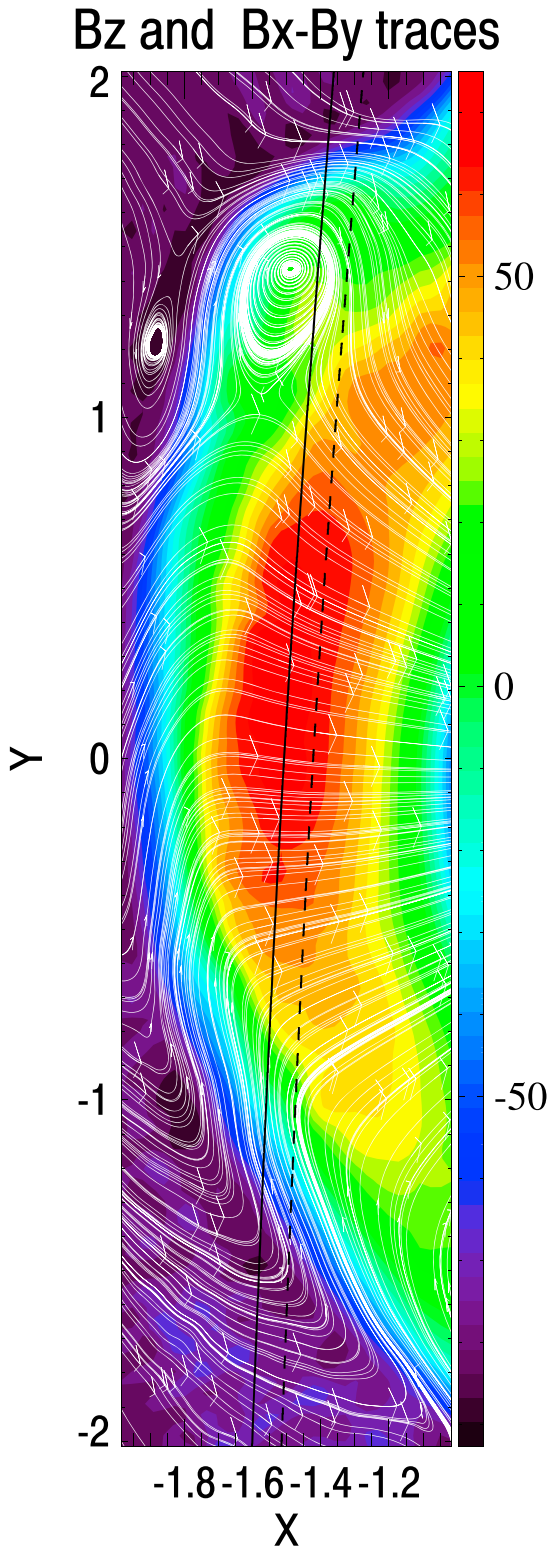

Figure 11. Cut plane at $z = 0.83\ R_G$ through the MHD-EPIC simulation at time $t_{sim} = 190$ s. The colors show the out-of-plane magnetic field component B_z. The white lines follow the B_x and B_y components. The dashed black line is the projection of the original Galileo trajectory, while the solid line is the stretched trajectory used to extract the data for Figure 10. The modified trajectory goes through the middle of an FTE near the outbound crossing of the magnetopause. The spacecraft moved toward the positive Y direction.

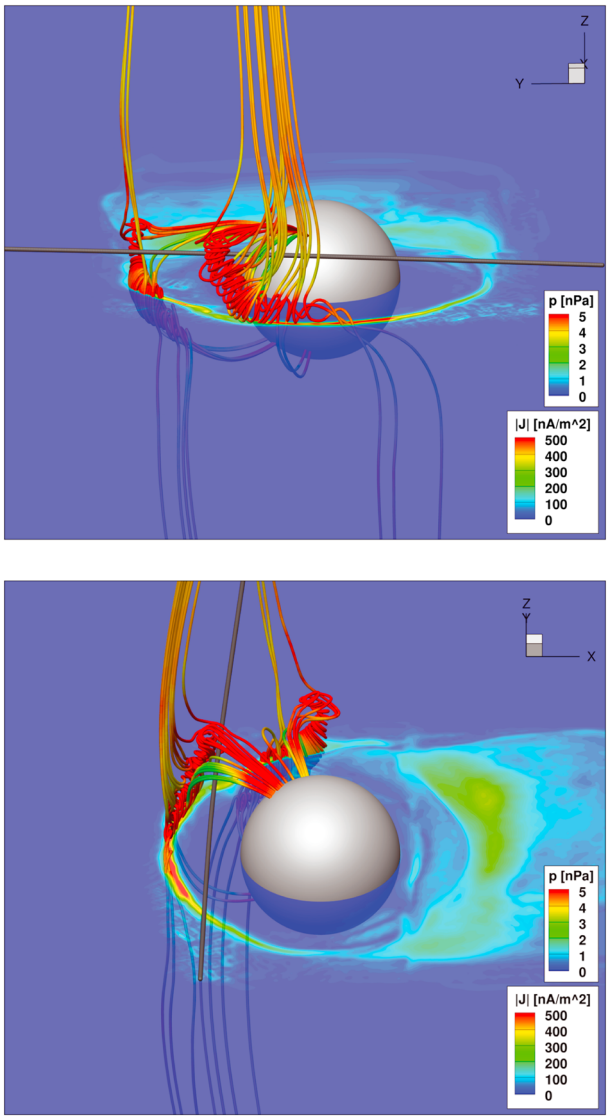

Figure 12. 3-D visualization of the magnetic field structure from the (top) $-X, +Z$ and (bottom) $-Y, +Z$ directions obtained by the MHD-EPIC simulation at time $t_{sim} = 190$ s. The almost straight gray tube indicates the Galileo trajectory. The colored tubes show selected magnetic field lines colored by the pressure. The translucent equatorial plane is colored with the current density. Ganymede's surface is shown by the gray sphere.

solution of this high-resolution simulation is quite similar to the coarser Hall MHD results. The out-of-plane B_y field remains similar to that shown in Figure 4 (left), with a slightly increased amplitude but still much narrower in the X direction than the MHD-EPIC solution shown in Figure 4 (right). The density inside the magnetosphere also remains lower than that for the MHD-EPIC solution, similar to the results shown in Figures 6 and 7. On the other hand, the solution became much more dynamic at this twice higher grid resolution, and the Hall MHD simulation shows FTEs on the upstream side as well as repeated plasmoid formation in the tail. The magnetic field extracted along the Galileo orbit shows dynamic features both at the inbound and outbound times. The fast Fourier transform (FFT) power spectrum of the extracted synthetic magnetic field observation is very similar to the Galileo data. We conclude that the small-scale features of the Hall MHD results are sensitive to the grid resolution. We note that the high-resolution Hall MHD simulation was much more expensive than the original simulation, and it required 4.9 h on 1920 cores or about 9500 core hours to model 1 min of simulation time, which is about 16 times more than the coarser run.

We also did a Hall MHD-EPIC simulation using a single upstream PIC region with 1/64 R_G grid resolution, so the $112 \times 368 \times 300$ grid consist of about 12 million cells. To reduce the memory used by iPIC3D, the number

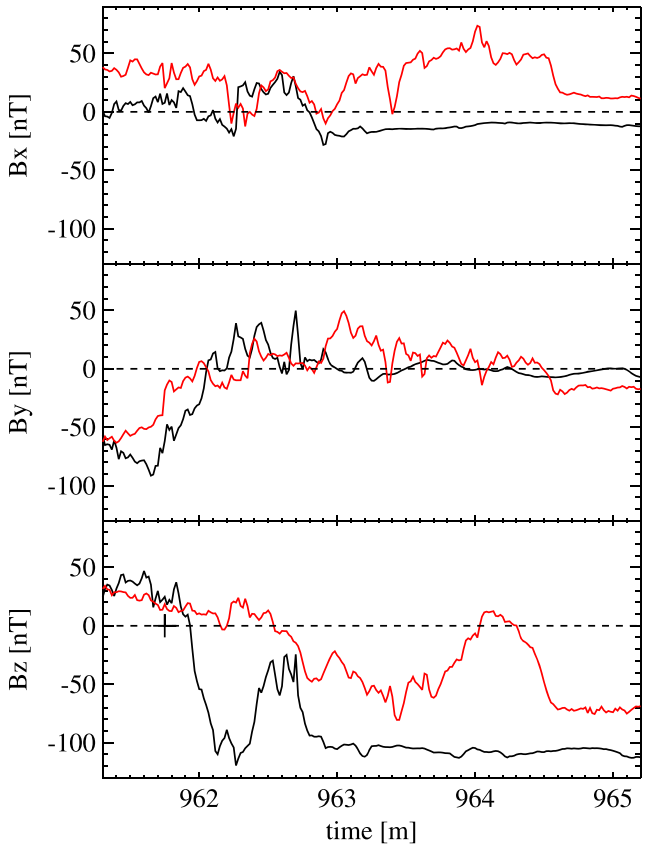

Figure 13. Comparison of the observed (black line) and Hall MHD-EPIC (red line) magnetic fields near the outbound magnetopause crossing. The cross at 961.75 min in the bottom panel shows where the simulation time jumps from 600 s back to 60 s, which is outside the event. The observed and simulated fields show clear, and comparable, signature of flux transfer events (FTEs).

of macroparticles was set to 125 ions and 125 electrons (instead of 216), so the total number of particles is about 3 billion initially. There are 8 times more grid cells and about 4.6 times more particles per unit volume than in the reference MHD-EPIC simulation, so the errors due to finite number of cells and particles in the PIC domain should reduce substantially. The time step had to be reduced to $\Delta t = 0.005$ s to maintain stability. The BATS-R-US grid was kept the same as in the baseline runs with 1/32 R_G cell size in the most refined part of the grid. This run demonstrates that the MHD-EPIC algorithm works even if the MHD and PIC grids are not the same. It also demonstrates that the PIC regions do not have to cover the whole magnetosphere to obtain a meaningful simulation. Even with these adjustments, the high-resolution run required about 24,000 core hours to simulate 1 min of simulation time (about 10 times more than the reference MHD-EPIC run). We found that the solution inside the upstream PIC region did not change significantly relative to the reference solution obtained with 1/32 R_G resolution. There are a few FTE-like events reminiscent of the observations, and the FFT spectrum remains close to the observations. Figure 15 shows a flux rope crossing the $Y = 0$ plane close to the equatorial plane similar to the flux rope obtained in the reference MHD-EPIC simulation shown in Figure 12. Note, however, that the helicity of this flux rope is positive and it bends toward $-Z$ for positive Y, while the flux rope in Figure 12 has a mostly negative helicity and bends toward $+Z$ for positive Y. Figure 16 shows the electron number density, magnetic field lines, and the direction of the electric field in the $Y = 0$ cut through the PIC region. The electron density is enhanced inside the flux rope. Figure 17 shows the electron and ion distribution functions obtained by iPIC3D in the vicinity of the flux rope. The phase space density is binned by the X coordinate and the three components of velocity both for electrons and ions. There is a significant electron heating inside the flux rope as shown by the enhanced width of the electron velocity distribution function near $x \approx 2.5$ Mm. The ion distribution function shows some anisotropy: the thermal widths of the X and Y components of the velocity are the largest and smallest, respectively.

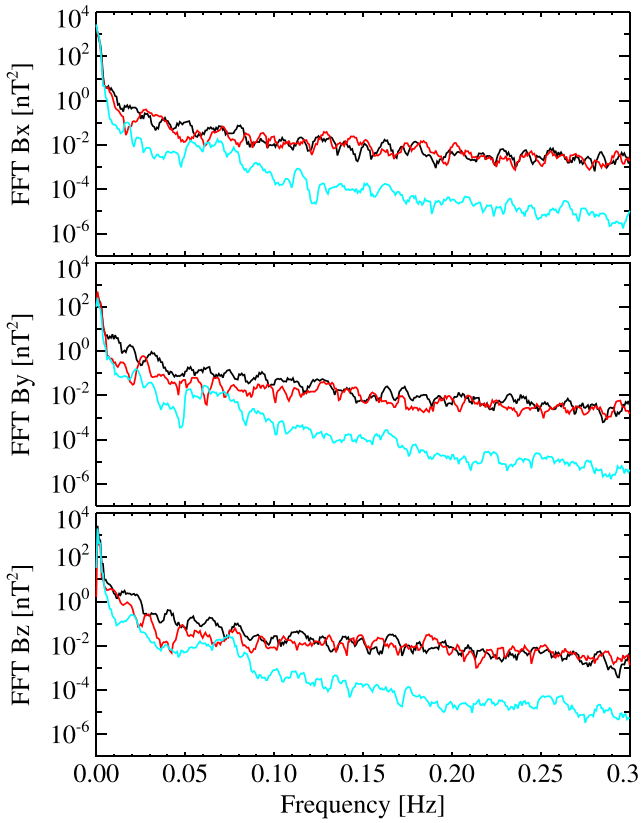

Figure 14. Power spectra of the observed (black), Hall MHD (blue), and MHD-EPIC (red) simulated components of the magnetic field. The frequency grid has a 0.75 mHz spacing. The spectra are smoothed over five frequency points for sake of clarity.

Galileo observations [*Kivelson et al.*, 2004] show that the Jovian plasma consists of a mixture of a thermal population and a hot ion population. The number density is dominated by the thermal population, while the thermal pressure is dominated by the hot ions. Both populations are a mixture of hydrogen and oxygen ions. We performed an MHD-EPIC simulation using only the thermal ion population with the mass density $\rho = 56\ m_p/\mathrm{cm}^{-3}$, but the total Jovian wind pressure is set to $p_i = 0.2$ nPa (instead of 3.8 nPa) with $p_e = p_i/5$. The BATS-R-US grid was the same as in the reference MHD-EPIC simulation, but only two PIC regions were used: the upstream and tail regions with the 1/32 R_G grid resolution. To maintain stability, we had to reduce the time step to $\Delta t = 0.005$ s, which made this simulation more expensive than the reference MHD-EPIC simulation that used $\Delta t = 0.025$ s. The overall structure of the magnetosphere changes significantly due to the reduced thermal pressure of the incoming Jovian plasma. The magnetopause moved farther out because of the weaker upstream pressure, so we had to increase the stretch factor of the Galileo trajectory from 1.06 to 1.14. Even with this increased stretch factor the smooth part of the magnetic field does not agree too well with the observed fields because the field observed along the Galileo trajectory during this pass is very sensitive to both the size and the shape of the magnetosphere, which changes in response to variations of the upstream pressure. Nevertheless, the simulation produced a few FTEs that looked remarkably similar to the observed data as shown in Figure 18. This implies that the energy distribution of the Jovian plasma does not make a huge difference in the FTE formation. In the future, however, we plan to do simulations with separate hot and thermal ion components. This will require extending the coupler to multi-ion Hall MHD-EPIC.

Finally, we also examined what causes the strong bending of the flux rope as it extends from the equatorial plane up to the $Z = 0.8$ plane near the Galileo trajectory. The symmetry with respect to the equatorial plane is broken by the tilt of the internal dipole and the electric field caused by the B_y component of the incoming Jovian magnetic field. We performed a simulation with the dipole aligned with the Z axis and $B_y = 0$ for the Jovian magnetic field. Although this $\pm Z$ symmetric run also showed reconnection island formation in the $Y = 0$

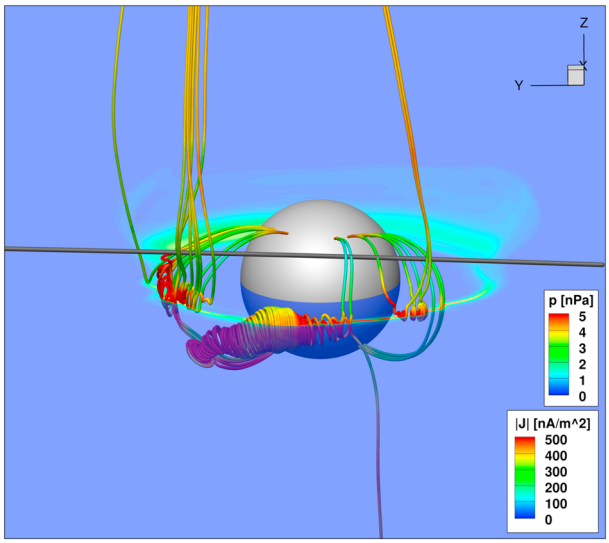

Figure 15. 3-D visualization of the magnetic field structure from the $-X, +Z$ direction obtained by the high-resolution MHD-EPIC simulation with a single PIC region with 1/64 R_G resolution at time $t_{sim} = 180$ s. The almost straight gray tube indicates the Galileo trajectory. The colored tubes show selected magnetic field lines colored by the pressure. The translucent equatorial plane is colored with the current density. Ganymede's surface is shown by the gray sphere.

plane, no extended flux ropes were formed. For this symmetric case the synthetic Galileo data do not show any FTE signatures, and the FFT power spectrum has a lower magnitude than what is observed. The simulations suggest that flux ropes are more likely to form with a guide field (B_y component), and the bending is most likely caused by the kink instability. We note, however, that the helicity of the flux rope is not determined by the B_y component in a straightforward manner. The simulations contain flux ropes with both positive and negative helicities.

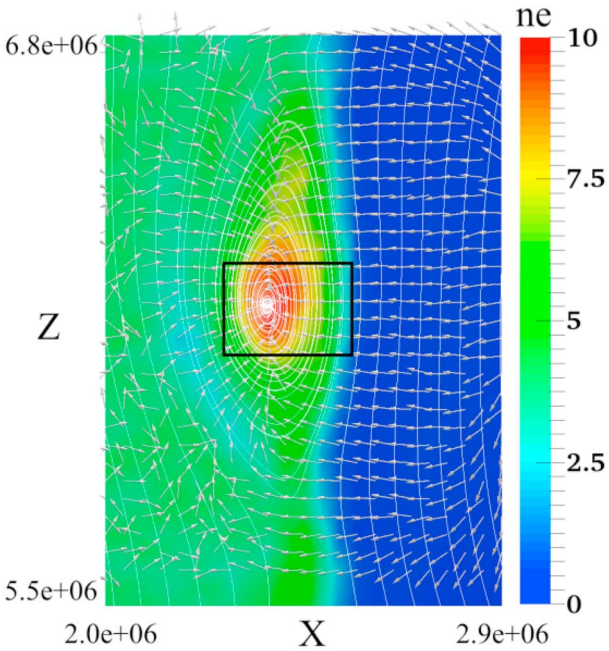

Figure 16. $Y = 0$ cut through the PIC region of the high 1/64 R_G resolution MHD-EPIC simulation at time $t_{sim} = 180$ s showing the electron number density (color contours) in units of cm^{-3}, the magnetic field lines (white lines), and the electric field directions (arrows). Coordinates are measured in meters relative to the corner of the PIC region. The black rectangle indicates the edges of the 3-D box 2.2 Mm $< x <$ 2.6 Mm, 7.45 Mm$< y <$7.75 Mm, 6.05 Mm$< z <$ 6.3 Mm from which the distribution functions in Figure 17 are obtained.

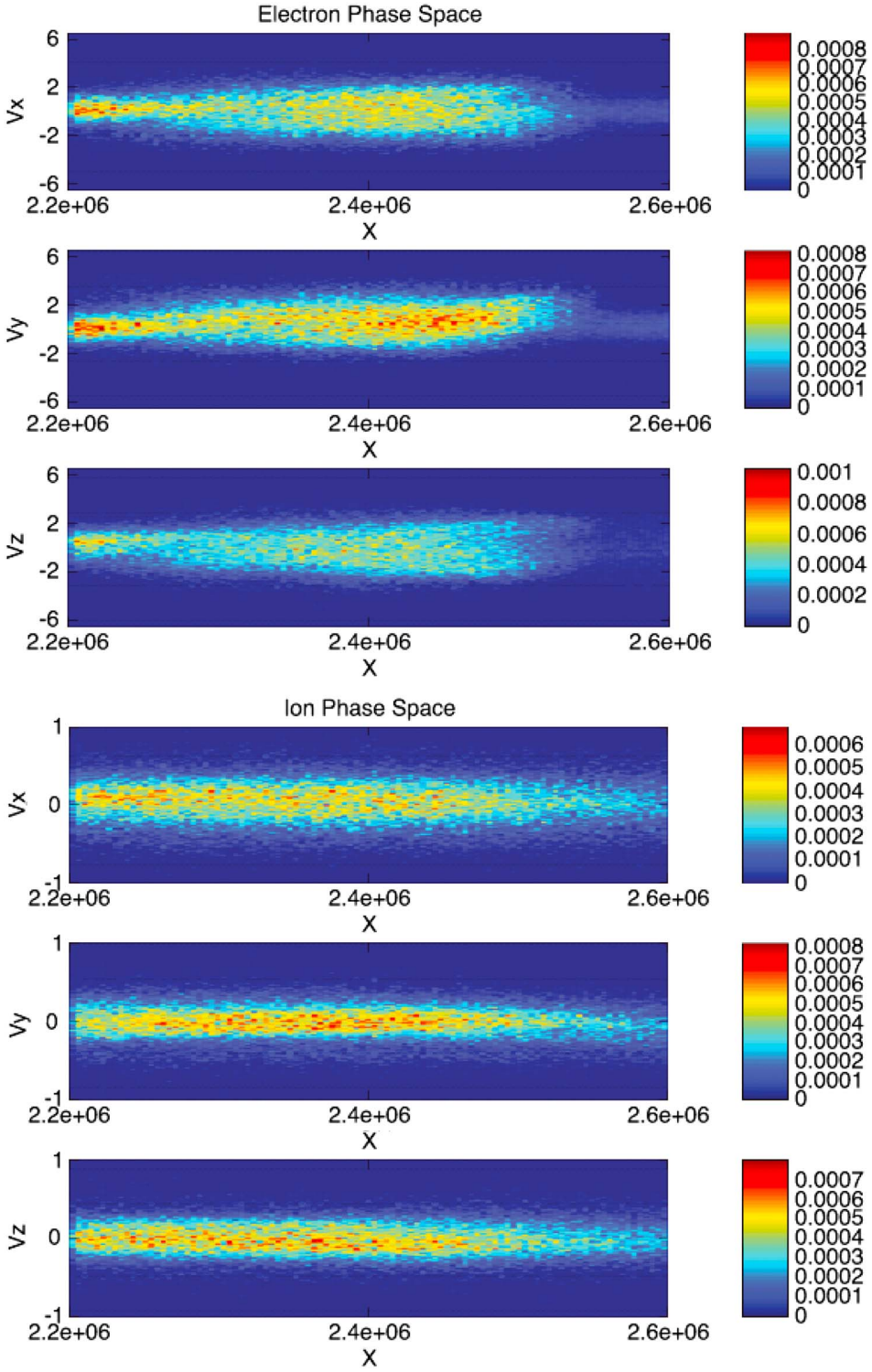

Figure 17. Electron and ion distribution functions binned by the *X* coordinate (measured in meters relative to the corner of the PIC region) and the three components of velocity (measured in Mm/s) in a box near the flux rope as shown in Figure 16. The electron and ion phases space densities are normalized so that their integral over the 3-D box and the velocity space is unity.

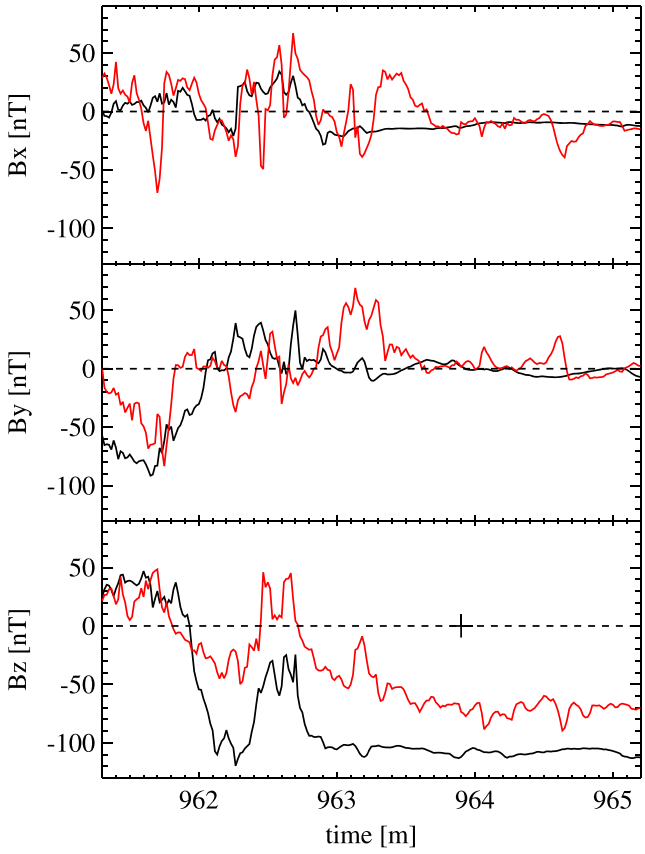

Figure 18. Comparison of the observed (black line) and Hall MHD-EPIC simulation with thermal Jovian ions only (red line) magnetic fields near the outbound magnetopause crossing. The cross at 963.9 min in the bottom panel shows where the simulation time jumps, which is clearly after the event. The observed and simulated fields show clear, and comparable, signatures of flux transfer events (FTEs).

5. Conclusion

We have successfully modeled Ganymede's magnetosphere with the new two-way coupled MHD-EPIC model. The embedded PIC regions fully covered the parts of the system where kinetic effects are likely to be important, so in effect we have produced the first fully kinetic and reasonably well-resolved numerical model of a global magnetosphere. The role of the Hall MHD model (driven by the Jovian wind values at the distant outer boundaries) is to calculate the proper boundary conditions for the PIC model and to properly propagate away the perturbations generated by the PIC model. In addition, the Hall MHD code also couples the four PIC regions together, because currently, we cannot use a single continuous PIC region to cover all the reconnection sites due to the limitations of the PIC grid (Cartesian box) and the presence of the moon in the middle. Since most of the interesting dynamics is happening inside the upstream PIC region and since there are no obvious numerical artifacts between the PIC regions, we are fairly confident that the results are not strongly affected by this approximation. In the future, however, we plan to improve the scheme by implementing direct communication between the PIC regions.

Our simulations show that the Hall MHD-EPIC model can simulate the dynamics of Ganymede's magnetosphere for the relevant global time scales. The numerical scheme works robustly, and there are no significant numerical artifacts. In fact, the Hall MHD and Hall MHD-EPIC models provide remarkably similar solutions, which confirm the importance of ion scale physics that is captured by both models (but not by ideal MHD, see *Dorelli et al.* [2015]). The similarity also implies that the MHD-EPIC coupling algorithm works well, and there are no significant numerical artifacts. There are also significant differences that we attribute to the additional kinetic physics in the PIC model, such as finite Larmor radius effects and non-Maxwellian distribution functions. We find that the PIC model gives a more dynamic solution as evidenced by the quasiperiodic formation of large FTEs at the upstream magnetopause. In comparison the Hall MHD solution with the same grid

resolution is less dynamic in this region. The Hall MHD solution, on the other hand, shows very clear signs of the Kelvin-Helmholtz instability in one quadrant of equatorial plane. The Hall MHD-EPIC model also shows oscillations in the same region, but the wavelength and the amplitude are smaller. We also find significant differences in the density and pressure distributions near Ganymede.

Comparison with the magnetic measurements of the Galileo spacecraft shows that there is a slight difference of about 6% between the observed and modeled magnetopause distances. There can be various reasons for this, including changes in the upstream Jovian wind conditions during the flyby and the representation of the inner boundary at the surface of the moon as a simple absorbing body with a fixed radial magnetic field. We plan to improve the description of the inner boundary by modeling the moon as a layered finite conductivity body. We expect that letting the magnetic field propagate into the body will reduce the simulated magnetopause distance in agreement with observations. This approach has been successfully used for Ganymede [*Jia et al.*, 2008] and recently for Mercury [*Jia et al.*, 2015].

The MHD-EPIC simulation produced an FTE that shows good agreement with the Galileo observations. The temporal width, the shapes, and magnitudes of the magnetic signatures in the three components of the magnetic field all resemble surprisingly well the observed FTE signatures. We only had one free parameter that could be adjusted, the relative time shift between the simulation and the observations. Looking at the 3-D structure of the FTEs reveals that the flux ropes can bend significantly and therefore exhibit complex magnetic geometries. Near the equatorial plane the flux ropes are roughly aligned with the Y axis, but near the Galileo trajectory at $Z \approx 0.8\,R_G$ the same flux rope can be more or less aligned with the Z axis. This means that the interpretation of the in situ magnetic measurements is not straightforward at all. The comprehensive 3-D MHD-EPIC model can provide the context and strongly suggest that Galileo observed an FTE indeed.

We also calculated the power spectra of the three magnetic components and found that the spectra of the observed and MHD-EPIC simulated fields are very similar, while the Hall MHD spectra deviate significantly with much less power in the higher frequencies. Increasing the grid resolution significantly improved the agreement with small-scale fluctuations for the Hall MHD model, but it did not make much difference for the MHD-EPIC model.

The embedded kinetic model can provide detailed information about the electron and ion distribution functions. Figure 17 demonstrates this capability and shows that there is significant heating inside the flux rope as also predicted by pure kinetic, mostly 2-D, simulations [*Drake et al.*, 2006]. We defer the more detailed analysis to a future publication.

Finally, we provide some information on the computational efficiency. All simulations (with the exception of the high-resolution Hall MHD run) were done on 960 CPU cores. For the standard grid simulating 1 min of physical time takes about 0.3 h wall clock time for resistive MHD, 0.6 h for Hall MHD, and 2.4 h for MHD-EPIC. If we tried to simulate the whole $(256\,R_G)^3$ domain with iPIC3D using the same 1/32 R_G grid resolution, it would require 500 billion PIC grid cells with 237 trillion macroparticles. Even assuming perfect parallel scaling, it would take about 20,000 CPU core years (not hours) to simulate a single minute of physical time, which is clearly not feasible and/or economical.

Our model is the first global kinetic model of a complete magnetosphere, but of course there are still some simplifications. In the Hall MHD model the Jovian wind was assumed to have a Maxwellian distribution and the electron pressure was taken to be one fifth of the ion pressure. In the future we will do runs where we distinguish between the thermal and hot ion populations and solve for the electron pressure in the Hall MHD model and couple it with iPIC3D. Direct coupling between the PIC regions will also be implemented. The representation of the inner boundaries will be improved by using a resistive body.

Acknowledgments
G.T. was partially supported by the Space Hazards Induced near Earth by Large, Dynamic Storms (SHIELDS) project DE-AC52-06NA25396, funded by the U.S. Department of Energy through the Los Alamos National Laboratory Directed Research and Development program and also by the INSPIRE NSF grant PHY-1513379. X.J. acknowledges support by the NASA Solar System Workings program through grant NNX15AH28G and the Heliophysics Supporting Research program through grant NNX15AJ68G. Computational resources supporting this work were provided by the NASA High-End Computing (HEC) Program through the NASA Advanced Supercomputing (NAS) Division at Ames Research Center and from Yellowstone (ark:/85065/d7wd3xhc), provided by NCAR's Computational and Information Systems Laboratory, and sponsored by the National Science Foundation. The SWMF code (including BATS-R-US and iPIC3D) is publicly available through the csem.engin.umich.edu/tools/swmf website after registration. The output of the simulations presented in this paper can be obtained by contacting the first author G.T.

References

Daldorff, L. K. S., G. Toth, T. I. Gombosi, G. Lapenta, J. Amaya, S. Markidis, and J. U. Brackbill (2014), Two-way coupling of a global Hall magnetohydrodynamics model with a local implicit particle-in-cell model, *J. Comput. Phys.*, *268*, 236–254, doi:10.1016/j.jcp.2014.03.009.

Dedner, A., F. Kemm, D. Kröner, C. Munz, T. Schnitzer, and M. Wesenberg (2003), Hyperbolic divergence cleaning for the MHD equations, *J. Comput. Phys.*, *175*, 645–673.

Dorelli, J. C., A. Glocer, G. Collinson, and G. Toth (2015), The role of the hall effect in the global structure and dynamics of planetary magnetospheres: Ganymede as a case study, *J. Geophys. Res. Space Physics*, *120*, 5377–5392, doi:10.1002/2014JA020951.

Drake, J. F., M. Swisdak, H. Che, and M. A. Shay (2006), Electron acceleration from contracting magnetic islands during reconnection, *Nature*, *443*, 553–556, doi:10.1038/nature05116.

Duling, S., J. Saur, and J. Wicht (2014), Consistent boundary conditions at nonconducting surfaces of planetary bodies: Applications in a new Ganymede MHD model, *J. Geophys. Res. Space Physics*, *119*, 4412–4440, doi:10.1002/2013JA019554.

Jia, X. (2015), Satellite magnetotails, in *Magnetotails in the Solar System, Geophys. Monogr. Ser.*, edited by A. Keiling, C. M. Jackman, and P. A. Delamere, John Wiley, Hoboken, N. J., doi:10.1002/9781118842324.ch8.

Jia, X., R. J. Walker, M. G. Kivelson, K. K. Khurana, and J. A. Linker (2008), Three-dimensional MHD simulations of Ganymede's magnetosphere, *J. Geophys. Res.*, *113*, A06212, doi:10.1029/2007JA012748.

Jia, X., R. J. Walker, M. G. Kivelson, K. K. Khurana, and J. A. Linker (2009), Properties of Ganymede's magnetosphere inferred from improved three-dimensional MHD simulations, *J. Geophys. Res.*, *114*, A09209, doi:10.1029/2009JA014375.

Jia, X., R. J. Walker, M. G. Kivelson, K. K. Khurana, and J. A. Linker (2010), Dynamics of Ganymede's magnetopause: Intermittent reconnection under steady external conditions, *J. Geophys. Res.*, *115*, A12202, doi:10.1029/2010JA015771.

Jia, X., J. A. Slavin, T. I. Gombosi, L. K. S. Daldorff, G. Toth, and B. van der Holst (2015), Global MHD simulations of Mercury's magnetosphere with coupled planetary interior: Induction effect of the planetary conducting core on the global interaction, *J. Geophys. Res. Space Physics*, *120*, 4763–4775, doi:10.1002/2015JA021143.

Kivelson, M., K. Khurana, F. Coroniti, S. Joy, C. Russell, R. Walker, J. Warnecke, L. Bennett, and C. Polanskey (1997), Magnetic field and magnetosphere of Ganymede, *Geophys. Res. Lett.*, *24*, 2155–2158.

Kivelson, M. G., J. Warnecke, L. Bennett, S. Joy, K. Khurana, J. A. Linker, C. Russell, R. J. Walker, and C. Polanskey (1998), Ganymede's magnetosphere: Magnetometer overview, *J. Geophys. Res.*, *103*(E9), 19,963–19,972, doi:10.1029/98JE00227.

Kivelson, M. G., K. K. Khurana, and M. Volwerk (2002), The permanent and inductive magnetic moments of Ganymede, *Icarus*, *157*, 507–522.

Kivelson, M. G., F. Bagenal, F. M. Neubauer, W. Kurth, C. Paranicas, and J. Saur (2004), Magnetospheric interactions with satellites, in *Jupiter: The Planet, Satellites and Magnetosphere*, edited by F. Bagenal, T. E. Dowling, and W. B. McKinnon, pp. 513–536, Cambridge Univ. Press, Cambridge, U. K.

Kopp, A., and W.-H. Ip (2002), Resistive MHD simulations of Ganymede's magnetosphere 2. Time variabilities of the magnetic field topology, *J. Geophys. Res.*, *107*(A12), 1490, doi:10.1029/2001JA005071.

Lapenta, G., S. Markidis, A. Divin, M. Goldman, and D. Newman (2010), Scales of guide field reconnection at the hydrogen mass ratio, *Phys. Plasmas*, *17*(8), 082106, doi:10.1063/1.3467503.

Liljeblad, E., T. Sundberg, T. Karlsson, and A. Kullen (2014), Statistical investigation of Kelvin-Helmholtz waves at the magnetopause of Mercury, *J. Geophys. Res. Space Physics*, *119*, 9670–9683, doi:10.1002/2014JA020614.

Markidis, S., G. Lapenta, and Rizwan-Uddin (2010), Multi-scale simulations of plasma with iPIC3D, *Math. Comput. Simul.*, *80*, 1509–1519, doi:10.1016/j.matcom.2009.08.038.

Neubauer, F. M. (1998), The sub-Alfvénic interaction of the Galilean satellites with the Jovian magnetosphere, *J. Geophys. Res.*, *103*, 19,843–19,866, doi:10.1029/97JE03370.

Paty, C., and R. Winglee (2004), Multi-fluid simulations of Ganymede's magnetosphere, *Geophys. Res. Lett.*, *31*, L24806, doi:10.1029/2004GL021220.

Paty, C., W. Paterson, and R. Winglee (2008), Ion energization in Ganymede's magnetosphere: Using multifluid simulations to interpret ion energy spectrograms, *J. Geophys. Res.*, *113*, A06211, doi:10.1029/2007JA012848.

Powell, K., P. Roe, T. Linde, T. Gombosi, and D. L. De Zeeuw (1999), A solution-adaptive upwind scheme for ideal magnetohydrodynamics, *J. Compt. Phys.*, *154*, 284–309.

Powell, K. G. (1994), An approximate Riemann solver for magnetohydrodynamics (that works in more than one dimension), *Tech. Rep. 94-24,* Inst. for Comput. Appl. in Sci. and Eng., NASA Langley Space Flight Center, Hampton, Va.

Ricci, P., G. Lapenta, and J. U. Brackbill (2002), Gem reconnection challenge: Implicit kinetic simulations with the physical mass ratio, *Geophys. Res. Lett.*, *29*(23), 2088, doi:10.1029/2002GL015314.

Tóth, G., et al. (2005), Space weather modeling framework: A new tool for the space science community, *J. Geophys. Res.*, *110*, A12226, doi:10.1029/2005JA011126.

Tóth, G., D. L. De Zeeuw, T. I. Gombosi, and K. G. Powell (2006), A parallel explicit/implicit time stepping scheme on block-adaptive grids, *J. Comput. Phys.*, *217*, 722–758, doi:10.1016/j.jcp.2006.01.029.

Tóth, G., Y. J. Ma, and T. I. Gombosi (2008), Hall magnetohydrodynamics on block adaptive grids, *J. Comput. Phys.*, *227*, 6967–6984, doi:10.1016/j.jcp.2008.04.010.

Tóth, G., et al. (2012), Adaptive numerical algorithms in space weather modeling, *J. Comput. Phys.*, *231*, 870–903, doi:10.1016/j.jcp.2011.02.006.